The Journal of Experimental Biology 205, 627–639 (2002)
Printed in Great Britain © The Company of Biologists Limited 2002
JEB3815



# Kinematics and hydrodynamics of an invertebrate undulatory swimmer: the damsel-fly larva

John Brackenbury*

*Department of Anatomy, University of Cambridge, Downing Street, Cambridge CB2 3DY, UK*

*e-mail: jhb1000@cam.ac.uk

*Accepted 10 December 2001*

## Summary

**The kinematics and hydrodynamics of free-swimming larvae of *Enallagma cyathigerum* were investigated using videography combined with a simple wake visualisation technique (tracer dyes). Damsel-fly larvae are undulatory swimmers with two distinct styles of movement: 'slow' swimming, in which body undulation is assisted by paddling of the legs, and 'fast' swimming, in which the legs are inactive. In both cases, the wake consists of discrete ring vortices shed from the caudal fin at the end of each half-stroke. The vortices propagate away from the mid-line, alternately to one side of the body then the other, at an angle of 67° from dead aft. There is no aft-flowing jet such as that observed in the wakes of continuously swimming fish that use caudal fin propulsion. The estimated momentum within the vortices, and the resultant thrust on the body are in tolerable agreement with calculations based on the large-amplitude bulk momentum model of fish locomotion. However, the drag on the body is not known, so it cannot be concluded with certainty that a force balance exists. The agreement between experiment and prediction gives confidence to the idea that most, if not all, of the vorticity generated by the swimming larva is located within the observable wake elements.**

Key words: larva, swimming, caudal fin, kinematics, vortex wake, hydromechanical model, starting manoeuvre, damsel-fly, *Enallagma cyathigerum*.

## Introduction

The precise manner in which swimming organisms generate propulsive force from the fluid medium surrounding them depends on, amongst other things, their size, shape, speed of locomotion and the style of bodily movements employed. As Lighthill (1969) states, most animals with an elongated body form use undulatory motion to propel themselves through the water. Amongst invertebrates (excluding micro-organisms), undulatory motion occurs in nematode worms (Gray and Lissman, 1964), leeches (Kristan et al., 1982), ascidian tadpoles (Chia et al., 1984), lancelet larvae (Stokes, 1997), ceratopogonid fly larvae (Nachtigall, 1961) and chironomid pupae (Brackenbury, 2000), although other aquatic insect larvae and pupae may use non-sinusoidal movements (Nachtigall, 1961, 1962, 1963; Brackenbury, 1999, 2000). Although Lighthill (1971) argues that most invertebrates swimming at intermediate Reynolds numbers (1–1000) are likely to depend mainly on the viscosity of the water to generate thrust, there is some evidence to the contrary. A hydromechanical model of chaetognath swimming (Jordan, 1992) explicitly takes into account inertial forces, although at present there appears to be little or no experimental evidence regarding the nature of the flow field in the vicinity of any invertebrate undulatory swimmer. Such data are necessary to offer at least some clue as to the way in which the wake could be modelled and, from this, the amount of momentum injected into the water could be estimated.

Much greater progress has been made in matching observations to model predictions in flying birds and insects and in swimming fish. Flow visualisation studies in flying insects (for a review, see Grodnitsky, 1999), birds (Spedding et al., 1984; Spedding, 1986, 1987) and bats (Rayner et al., 1986) suggest that the vortex models formulated by Rayner (1979) and Ellington (1984) provide an accurate description of the way in which energy is organised in the wakes of moving animals. The essence of these theories is that bursts of vorticity released by the propulsor should be composed of closed vortex loops in the form of small-cored vortex rings although, in flying birds at least, there is a momentum deficit in the wake which may be accountable to structures that fail to show up in the visualisation process (Spedding, 1987). As Drucker and Lauder (1999) caution, any small inaccuracies of modelling of wake morphology will inevitably lead to errors in trying to match thrust production to the force required to drive the body forward (and if necessary to support its weight in the medium).

Wake visualisation studies using the methods of digital particle image velocimetry (Blickhan et al., 1992; Muller et al., 1997; Wolfgang et al., 1999; Drucker and Lauder, 1999, 2000) or thermal stratification (McCutchen, 1977) demonstrate that swimming fish also transfer momentum into the water in the form of regulated bursts of vorticity, although the three-dimensional structure of the wake depends on the speed and

swimming style. As Videler (1993) postulated, the wake generated by the caudal fin of a continuously swimming fish consists of a chain of linked ring vortices (Muller et al., 1997; Wolfgang et al., 1999), but use of the pectoral fins during slow swimming (Drucker and Lauder, 1999) or turning (Drucker and Lauder, 2000) in bluegill sunfish *Lepomis macrochirus* results in the production of discrete, unlinked vortices.

Other, less-refined methods than digital particle image velocimetry can be used to obtain information on the wakes of swimming organisms, but they may be difficult to quantify or practically beyond interpretation if the wake structure is highly complex. Using a dye tracer technique, it was possible to show that the wake of swimming mosquito larvae and pupae is relatively simple in structure, consisting of a series of discrete ring vortices shed to the right and left of the swimming line with alternate half-strokes (Brackenbury, 2001a). Calculations showed an approximate balance between the momentum imparted to the water and to the body with each half-stroke. Whilst culicids are not undulatory swimmers, and therefore do not address the problem outlined by Lighthill (1969, 1971) directly, their swimming demonstrates that inertial forces can dominate in invertebrate swimmers, even at low to intermediate Reynolds numbers (up to $10^3$). The present study advances this line of enquiry one step further by examining the kinematics and wake structure of an invertebrate that displays fish-like propulsion, the damsel-fly larva. Thrust values estimated from wake measurements compared favourably with those predicted from the kinematics using the large-amplitude, bulk-momentum model of undulatory swimming.

## Materials and methods

### *Animals and experimental techniques*

Larvae of *Enallagma cyathigerum* L. were collected from a permanent fresh-water pond the depth of which remained at least 1 m throughout the year, in the Willingham Fen district of northwest Cambridgeshire. Larvae with an approximate body length of 2 cm were selected by eye and transferred to an indoor tank at room temperature (approximately 18–22 °C), which was somewhat warmer than the mean outdoor temperature at the time of year (summer through to winter). Individuals were used within a few days of capture and were supplied with food in the form of small fly larvae, cladocerans and copepods. Swimming was filmed in daylight conditions using a Panasonic video camera (S-VHS format, horizontal resolution >400 lines at 25 frames $s^{-1}$) delivering 50 fields $s^{-1}$ (horizontal resolution of each field >200 lines) at shutter speeds of 0.001–0.0002 s. Video tapes were viewed on a cassette recorder with a single-field advance facility allowing detailed examination of kinematic and hydrodynamic events. Swimming trajectories and dye movements were traced by hand directly from the video screen.

During an experiment, two or three individuals were placed in a transparent container measuring 16 cm×8 cm×8 cm (width×depth×height) containing water to a depth of approximately 6–7 cm. The method of flow visualisation follows that described previously (Brackenbury, 2001a) and made use of tracer dyes consisting of a harmless food-colouring agent (E122) suspended in water and glycerol (specific gravity of suspension 1.012 g $ml^{-1}$) or fresh cows' milk. Two sets of experiments were designed which took account of the characteristic swimming behaviour of the larvae. Both in the wild and in the laboratory, *Enallagma cyathigerum* larvae prefer to live near the bottom of the water and, in accordance with this lifestyle, their bodies are denser than water. An inactive larva placed in mid-water, or suddenly ceasing to swim in mid-water, sinks with its longitudinal axis held horizontally and its legs partially extended in the resting position, at a speed of 2.1±0.3 cm $s^{-1}$ (mean ± S.D., $N$=12), approximately 13 % of the forward speed achieved during fast swimming (see Results). Locomotory behaviour was broadly of two kinds: horizontal swimming, with the body held just clear (by approximately 0.25–0.5 body length) of the bottom; and open-water swimming which could be downwards, upwards or horizontal.

In the first set of experiments, a thin layer (approximately 1 mm) of tracer was carefully laid down on the bottom of the container through a syringe, and larvae swimming across the bottom left behind a trail of 'foot-prints' as evidence of their wakes. These trails were filmed from directly above the container, care being taken to reject any trails in which there was evidence of direct contact between the body and the tracer. In practice, this distinction was easy to make since the wake-induced disturbance of the tracer during a 'clean run' across the bottom lagged behind the motion of the body itself by approximately 20–40 ms.

Although bottom-swimming is probably a normal form of locomotory behaviour in these larvae, from a methodological point of view, the bottom-layer technique is extremely limited and can only give an impression of the possible morphology of the wake. Apart from boundary conditions, which probably distort the wake compared with its open-water configuration, the bottom-layer method can only produce a two-dimensional impression of a three-dimensional wake structure. A more accurate technique was used to investigate open-water swimming by dispensing tracer into the water in the form of a narrow (approximately 0.5–1.0 mm) vertical streamer released from the barrel of a plungerless syringe mounted above the water, with the tip of its needle just penetrating the surface, and discharging slowly under the force of gravity. The speed of descent of the streamer throughout the water was only a fraction of the speed of the currents produced in the wakes of the insects. In total, approximately 80–100 individuals were used to collect data in both sets of experiments. Results are presented as mean values ±1 S.D.

### *Quantitative methods*

Independent methods were used to quantify thrust from the flow field and kinematic measurements respectively. Both methods assume that the thrust results from the acceleration of the water by the locomotory movements of the body, and any contribution from resistive forces is ignored. Whilst this

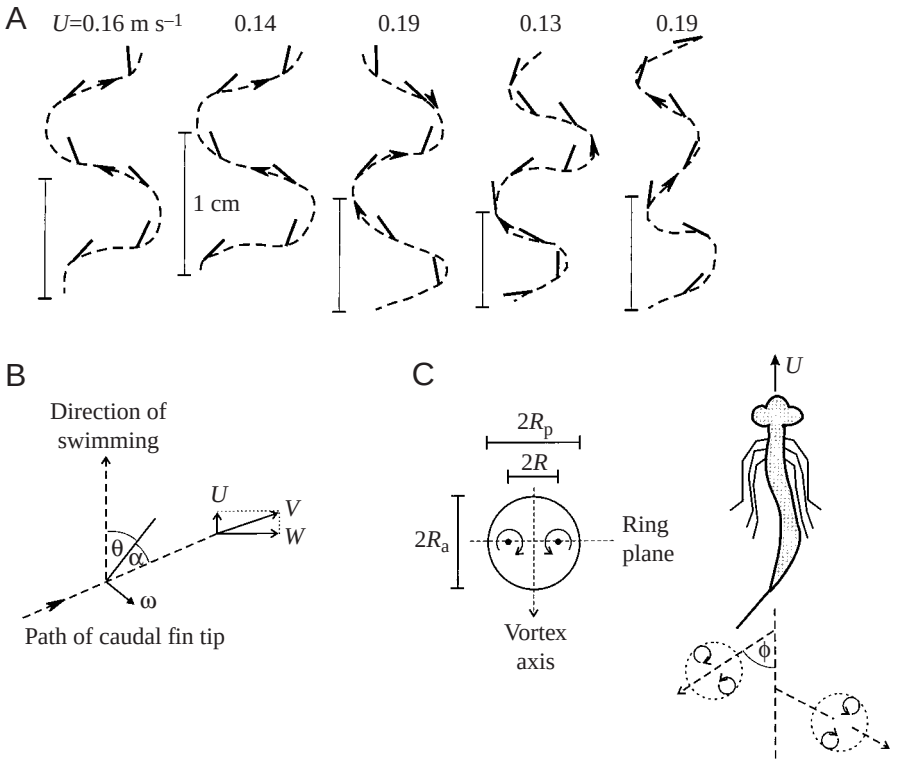


Fig. 1. (A) Paths traced out by the tip of the caudal fin during fast swimming in five damsel-fly larvae. Solid bars on the paths represent the orientation of the caudal fin. (B) Parameters used in the hydromechanical model (see text for details). α, angle of incidence of the tail fin to the instantaneous line of travel of the fin tip; θ, angle of inclination of the tail fin to the mean swimming line; ω, perpendicular velocity of the tail tip; *U*, instantaneous forward velocity; *V*, absolute velocity of the fin tip; *W*, lateral velocity of the tail tip. (C) Flow parameters used in the calculation of thrust from the vortices produced during fast swimming (see text for details). *R*, ring radius; $R_a$, external radius of the vortex measured along the axis; $R_p$, external radius of the vortex measured along the ring plane; ϕ, momentum angle of the jet measured in the frontal plane relative to dead aft of the swimming line.

assumption cannot be validated directly from the measurements available, it is at least partly justified by the whole-body Reynolds number of approximately $3\times10^3$. Thrust, thrust power and the kinematic energy of the wake were estimated using Lighthill's bulk-momentum model for large-amplitude, elongated-body fish locomotion (Lighthill, 1971). This model is preferable to the alternative model for small-amplitude swimming (Lighthill, 1969, 1970), although damsel-fly larvae are not ideal candidates since, although their propulsion is kinematically fish-like, their bodies are not bilaterally compressed, the condition that favours virtual mass enhancement. According to the large-amplitude model, the thrust force $F_T$ at any point in the swimming cycle can be calculated from:

$$F_T = m\omega W - \tfrac{1}{2}m\omega^2\cos\theta\,, \quad (1)$$

where ω and *W* are the perpendicular and lateral velocities of the tail tip, respectively (Fig. 1B), *m* is the virtual mass per unit length of the body and θ is the angle of inclination of the tail fin to the mean swimming line. ω and *W* are related to θ and to α, the angle of incidence of the tail fin to the instantaneous line of travel of the fin tip, and *V*, the absolute velocity of the fin tip, as follows:

$$\omega = V\sin\alpha\,, \quad (2)$$

$$W = V\sin(\alpha+\theta)\,. \quad (3)$$

*m* is given by:

$$m = \tfrac{1}{4}\pi\rho h^2\,, \quad (4)$$

where ρ is the density of water ($10^3$ kg m$^{-3}$) and *h* is the height of the trailing edge of the caudal fin.

The first term in equation 1 is the instantaneous thrust produced by the body wave, the second term is the pressure force due to loss of momentum to the wake. The rate of loss of kinetic energy to the wake averaged over the cycle $P_E$ is given as:

$$P_E = \tfrac{1}{2}m\omega^2 u\,, \quad (5)$$

where ω and *u*, the tangential velocity of the fin tip, are both averaged over the cycle. *u* can be calculated from the instantaneous forward velocity *U* as:

$$u = U\cos\theta\,. \quad (6)$$

Thrust power $P_T$ is calculated as the product of thrust and mean forward speed.

If the wake is found to consist of discrete axi-symmetric ring vortices, the momentum *M* of each of these can be estimated as:

$$M = \rho\pi R^2\Gamma\,, \quad (7)$$

where *R* is the ring radius and Γ is the circulation given by the line integral of the tangential velocity component *v* about a curve enclosing the vortex core (Spedding et al., 1984; Drucker and Lauder, 1999). From Spedding et al. (1984), Γ can be obtained by integrating *v* normal to the ring plane down the centre line of the vortex. Equation 7 assumes that the vortex meets the appropriate geometric criteria, i.e. that it is a small-cored ring vortex with a core radius to ring radius ratio of 0.25 or less. In the present study, it was only possible to obtain an estimate of the jet velocity at the ring plane $V_{jet}$, and the images of the vortices were not detailed enough to establish a profile of *v* along the vortex axis. However, in a previous study (Brackenbury, 2001a) of vortices produced in the wakes of

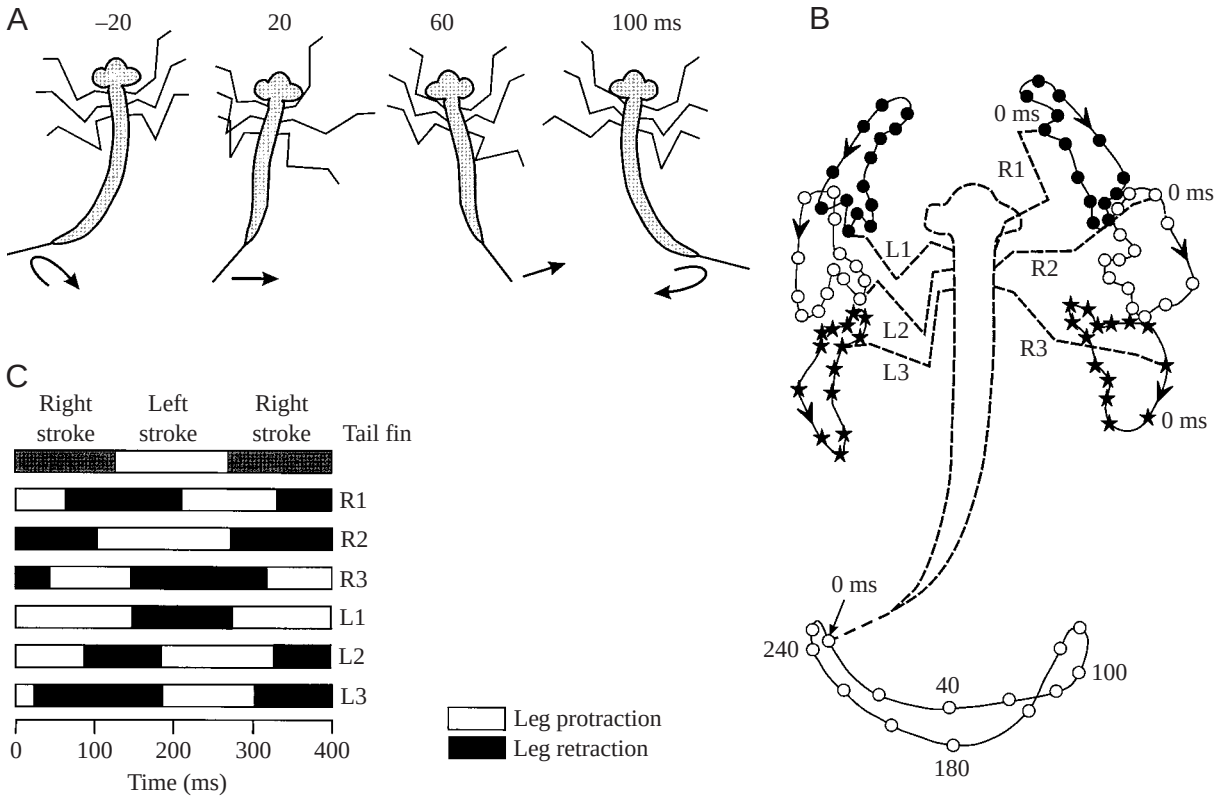


Fig. 2. Kinematics of body and leg movements during slow swimming. (A) Four stages in the left-to-right half-stroke of the caudal fin. The times are with reference to the zero position of the leg tips and fin tip shown in B. (B) Paths traced out by the caudal fin tip and the tips of the hindlimbs (stars), middle limbs (open circles) and forelimbs (filled circles) during a single swimming cycle. The limb tip paths are zeroed to the start of the left-to-right swing of the abdomen. Limb tip positions are drawn relative to the head. (C) Periods of protraction (open bars) and retraction (filled bars) of the limbs during three consecutive half-strokes of the caudal fin. L, left; R, right; 1, front leg; 2, middle leg; 3, hind leg.

swimming culicid pupae, the jet velocity was seen to regress more-or-less linearly from its maximum value at the ring plane, $V_{jet}$, to zero at the leading and trailing edges of the vortex. Knowing $V_{jet}$, it was then possible to estimate $\Gamma$ approximately as follows:

$$\Gamma = V_{jet} R_a , \quad (8)$$

where $R_a$ is the external radius of the vortex measured along the axis (Fig. 1C).

From equations 7 and 8, $M$ can then be expressed as:

$$M = \rho\pi R^2 V_{jet} R_a . \quad (9)$$

The mean force $F$ on the propulsor surface associated with the production of the vortex is equal to the mean rate of change of momentum within the vortex:

$$F = M/T , \quad (10)$$

where $T$ is the period of one half-stroke. The forward component of $F$, thrust, is given as:

$$F_T = F\cos\phi , \quad (11)$$

where $\phi$ is the momentum angle of the jet measured in the frontal plane, relative to dead aft of the swimming line (Fig. 1C).

The self-energy $E$ of the vortex can be calculated as:

$$E = \tfrac{1}{2}\rho\Gamma^2 R[\log_e(8R/R_o) + A - 2] \quad (12)$$

(Spedding et al., 1984), where $R_o$ is the core radius and the constant $A$, which is dependent on the distribution of vorticity across the core, was assigned a value of 0.25 by Spedding et al. (1984). When the core radius to ring radius ratio is less than 0.25, equation 12 reduces the approximate form:

$$E \approx \rho\Gamma^2 R . \quad (13)$$

This quantity, multiplied by the half-stroke rate $2F$, gives the rate of loss of kinetic energy to the wake $P_E$.

## Results

### *Kinematics and morphology*

Damsel-fly larvae use two kinds of swimming, both based on undulations of the body in the frontal plane but differing in speed and the auxiliary use of the legs. During ‘slow’ swimming (approximately 3 BL $s^{-1}$, where BL is body length), the legs perform a rowing motion that is independent of the undulatory wave but has the same frequency and is phase-linked to it. Relative to the head and thorax, each leg undergoes a cycle of protraction/flexion (the forward stroke) and retraction/extension (the backward stroke). Consequently,

Table 1. *Kinematic and hydrodynamic parameters of damsel-fly larvae during continuous 'fast' swimming*

| | |
|---|---|
| Body mass (mg) | 22 |
| Body length (cm) | 1.9±0.1 (8) |
| Swimming speed (cm $s^{-1}$) | 15.1±2.2 (25) |
| Swimming speed (BL $s^{-1}$) | 7.9±1.2 (25) |
| Stroke frequency ($s^{-1}$) | 13.8±1.6 (23) |
| Vortex ring diameter (cm) | 0.43±0.06 (51) |
| Vortex external diameter (cm) | 0.67±0.10 (51)[a] |
| Vortex jet velocity (cm $s^{-1}$) | 10.4±2.2 (37)[b] |
| Vortex momentum angle (degrees) | 67.4±14.0 (29)[c] |

Body mass was determined as the mean of eight animals weighed together.

BL, body length.

[a]Measured along the vortex axis; [b]measured at the ring plane; [c]measured in the frontal plane relative to dead aft.

Values are means ± S.D. (*N*).

viewed from the dorsal side, the tip of the leg traces out a roughly ellipsoidal path during each cycle, the long axis of the ellipse being roughly aligned with the mean line of travel of the body (Fig. 2A,B). The legs move in strict succession, the rhythm beginning in the left hind leg (L3) and moving progressively through L2, L1, R3, R2 and finally R1 (Fig. 2C). The metachronal movements of the legs thus follow the normal hexapod pattern of limb activation: hind, middle then fore (Hughes, 1974; Hoyle, 1976). The mean speed and stroke frequency were 5.7±1.7 cm $s^{-1}$ (*N*=12) and 4.3±0.4 $s^{-1}$ (*N*=20), approximately one-third of their corresponding values during 'fast' swimming (Table 1). In the latter case, the legs are trailed behind the body, in the maximally extended position, where it is assumed that they offer least resistance to the water (Fig. 1C).

The caudal fin is made up of the three tracheal plates, one median and dorsal, the other two lateral and ventral, that make up the abdominal gill (Fig. 3A). Each plate can be divided into a narrow basal segment stiffened by serrated ribs of sclerotin and a more flexible apical segment lacking any stiffening elements but bearing a fringe of long, flexible hairs (Fig. 3B). These two zones are sharply divided by a flexion line. The distribution of thickening elements varies between the median and lateral plates. The base of the median plate has a quadrangular cross section, and stiffening is distributed along each of the edges. The lateral plates are more triangular in section, with each of the three edges stiffened but lacking the equivalent of a median rib (Fig. 3A).

From the distribution of thickening elements alone, it could be conjectured that each of the lateral plates would be less resistant to deflection forces applied to its lateral side than to its median side. This assumption is supported by the behaviour of the fin elements during swimming. As soon as swimming commences, the lateral plates, which at rest diverge away from the mid-line, become pressed against the median plate, the three elements forming a single surface in the median plane. The exact disposition of the lateral elements influences the effective height of the fin. In the middle of the stroke, the three plates are splayed maximally from the base, forming a roughly three-plate-high surface, whilst towards the stroke extremes the lateral plates move into a back-to-back position, reducing the effective height of the fin to approximately two plate widths (Fig. 3C). These positional changes show that there is considerable mobility of the lateral plates within both the frontal and median planes.

The distribution of longitudinal stiffening in the lateral plates might explain how the three plates fold together in the median plane in response to hydrodynamic forces, but the fan-like, radial mobility of the plates in the vertical plane, which

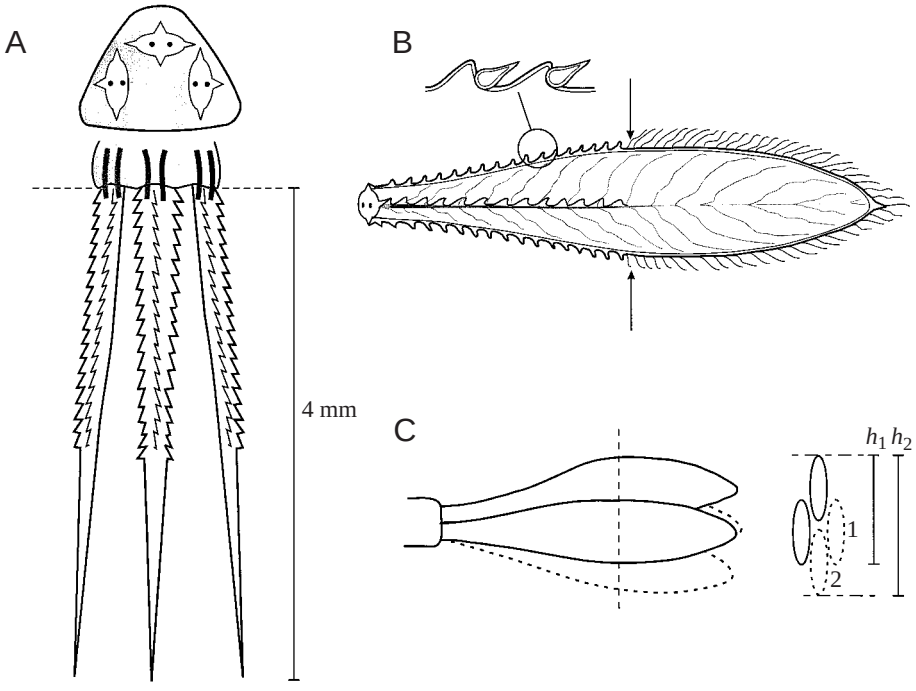


Fig. 3. Structure of the caudal fin of *Enallagma cyathigerum* larva. (A) Dorsal view of the end of the abdomen bearing the three tracheal plates. Each plate receives two trunks from the abdominal tracheal network. The inset shows a cross section of the abdominal tip. Note that the base of the median plate has a quadrangular section, that of the two lateral plates a triangular section, with thickening along the ridges. (B) Lateral view of the left lateral tracheal plate. The arrows point to the flexion line separating the stiffened basal segment from the apical segment. The inset shows that the serrated appearance of the stiffening ribs is due to the presence of a single row of stout setae. (C) Configuration of the tracheal plates during swimming. Throughout the cycle, the height (*h*) of the apex of the fin varies from approximately 2 plate widths (configuration 1) to 3 plate widths (configuration 2). The dashed line in the side view of the tail plates represents the location of the vertical section on the right.

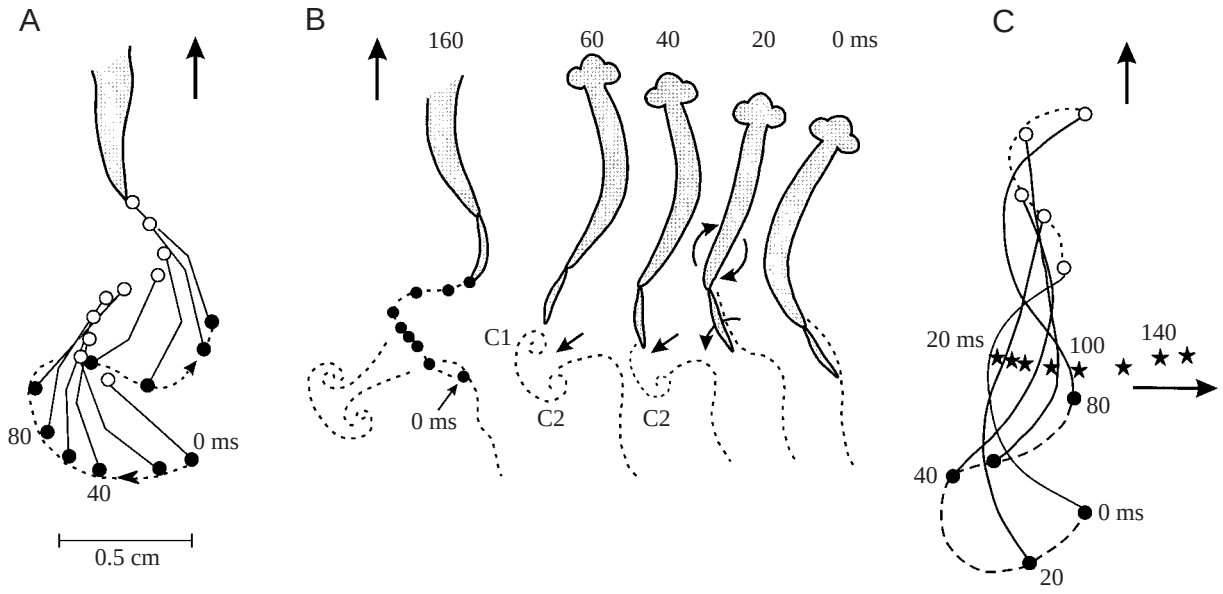


Fig. 4. (A) Configuration of the caudal fin during the stroke cycle. The end of the abdomen is viewed from above, and the open and filled circles trace the paths of the base and tip of the fin respectively. Note how the fin bends specifically along the flexion line dividing the basal and apical segments of the tracheal plates. (B) Consecutive stages in the production of a ring vortex during a single right-to-left half-stroke of a larva viewed from above. These profiles are taken from Fig. 8, but also plot the path of the fin tip during the right-to-left and the following left-to-right half-strokes (160 ms position, far left). Arrows in the flow field indicate the axis of the vortex jet and the body flow contributing to the proximal vortex (20 ms position). (C) Whole-body profiles of a swimming larva at 20 ms intervals. Open and filled circles plot the path of the head and fin tip respectively. The stars plot the motion of a portion of dye streamer carried progressively to the right by the movements of the body as the undulatory wave travels caudally. By the time the larva has moved to the 80 ms position, the body-induced motion of particles in the dye stream joins the vortex jet released from the tail, which travels laterally in the direction of the arrow.

underpins the cyclic variation in effective fin height, might be due to active forces operating from the base as well as to passive factors. The flexion line markedly affects the angle of attack adopted by the fin tip during the stroke, the fin being maximally flexed in the middle of the stroke and momentarily straightened at the stroke transitions (Fig. 4A). The mean deflection of the apical segment relative to the basal segment, measured over the middle range of the stroke, was 37.9±6.4° ($N$=28).

### *Hydromechanical modelling*

An example of the use of the hydromechanical model for calculating the thrust force from the kinematic measurements is shown in Fig. 5A. In both this figure and Fig. 1A, the angle of attack of the caudal fin refers to the apical segment. As is typical of slow swimming, the tip of the fin follows a sideways and slightly backwards course relative to the water during the stroke and is drawn almost directly forwards at the stroke transition. A peak in thrust production occurs in the middle of the stroke as the fin tip crosses the mid-line (Fig. 5B), whilst at the stroke transition, momentarily before it begins its excursion to the other side, the tip develops a negative angle of attack accompanied by a small reversal of thrust. As will be shown below, this moment coincides with the shedding of the ring vortex formed during the half-stroke. During fast swimming, the limited sampling frequency of data points precluded the kind of detailed force profile obtainable in slow swimming, so a mean value was estimated from the sum of the data points recorded over an integral number of half-cycles. This was performed for the five examples illustrated in Fig. 1A, care being taken to select sequences of straight swimming at constant speed.

In terms of kinematics, the main consequence of an increased forward speed was to eliminate the backward component of the motion of the fin tip relative to the water during the stroke so that the resultant fin tip path was essentially sinusoidal rather than zig-zag. Individual and overall mean values for thrust, thrust power, rate of loss of kinetic energy to the wake and propulsive efficiency are presented in the left-hand columns of Table 2. The limited data sampling frequency in these experiments will have reduced the accuracy of the values obtained for each individual, although this source of error will have been offset in the overall results. These estimates show that, during fast swimming, approximately one-third of the energy of the undulatory wave is lost to the wake, the remaining two-thirds being used to drive the body forwards against the drag of the water, the overall efficiency being 67 %. Note that this method takes no account of a lifting force that must be generated to support the larva against its own tendency to sink.

### *Wake measurements*

An example of the trail of impressions left in a thin layer of milk by the wake of a larva swimming at constant speed in ‘fast’ mode just above the bottom of the container is shown in Fig. 6. In the many cases (approximately 150–200) in which such trails were observed, the dominant impression was of an outward

Table 2. *Comparison of hydrodynamic variables estimated from experimental flow field recordings and hydromechanical model predictions*

| | Hydromechanical model | | | | | | Flow field |
|---|---|---|---|---|---|---|---|
| Animal: | A1 | A2 | A3 | A4 | A5 | Mean | |
| Swimming speed ($m\,s^{-1}$) | 0.13 | 0.19 | 0.14 | 0.16 | 0.19 | 0.16 | 0.15 |
| Thrust (N) | $12.5\times10^{-5}$ | $6.5\times10^{-5}$ | $15.0\times10^{-5}$ | $14.0\times10^{-5}$ | $15.0\times10^{-5}$ | $12.6\times10^{-5}$ | $10.0\times10^{-5}$ |
| Thrust power (J) | $1.6\times10^{-5}$ | $1.2\times10^{-5}$ | $2.0\times10^{-5}$ | $2.1\times10^{-5}$ | $2.9\times10^{-5}$ | $2.0\times10^{-5}$ | $1.5\times10^{-5}$ |
| Rate of kinetic energy loss to wake (J) | $0.7\times10^{-5}$ | $0.4\times10^{-5}$ | $1.0\times10^{-5}$ | $1.3\times10^{-5}$ | $2.0\times10^{-5}$ | $1.1\times10^{-5}$ | $0.8\times10^{-5}$ |
| Propulsive efficiency | 0.70 | 0.75 | 0.68 | 0.63 | 0.59 | 0.67 | 0.65 |

movement of water away from the mid-line, there being no evidence of an aft-flowing jet. The streak-lines suggest a sideways-travelling jet produced at the end of each half-stroke. In 63 individual trails obtained during constant-speed swimming, the momentum angle of the jet, in the frontal plane, was 71.5±14.8° relative to dead aft. This pattern was achieved by the end of the second stroke from a 'standing' start. At the start of spontaneous swimming, the first visible vortex, which usually coincided with the second half-stroke of the tail (see next section), had a momentum angle of 43.8±8.6° ($N$=15). The velocity of the jet relative to the surrounding stationary water, measured as close as possible to the mid-line, was 10.9±1.2 $cm\,s^{-1}$ ($N$=29), approximately 70–75% of the forward velocity of the body. The open-water swimming experiments confirmed that each half-stroke results in the generation of a discrete vortex that is convected away from the mid-line.

Fig. 7 shows an example of a vortex shed from the tail fin intercepting a dye streamer and gradually becoming outlined in the process. First the leading edge, then the trailing edge and finally the axis of the vortex become visible, in the latter case as dye is drawn from the trailing edge into the vortex. In this particular example, the location of the opposite cores of the vortex was already evident from dye that had been drawn into the vortex before it reached the streamer. In 37 instances, it was possible to measure the velocity of the jet at the ring plane $V_{jet}$ relative to the surrounding stationary water, and this measurement was usually made within 50 ms of the vortex being shed from the tail fin. The vortex momentum angle, in the frontal plane, could be established in 29 separate sequences of steady forward swimming. Both variables (Table 1) were tolerably close in value to those measured in the bottom-swimming experiments.

The time course of the formation and shedding of an individual vortex can be seen in Fig. 8. This depicts one of a number of occasions in which a larva swam directly in line with a streamer. In Fig. 8A, the larva is just about to begin a right-to-left half-stroke of the fin. The motion of the fin draws a current of water

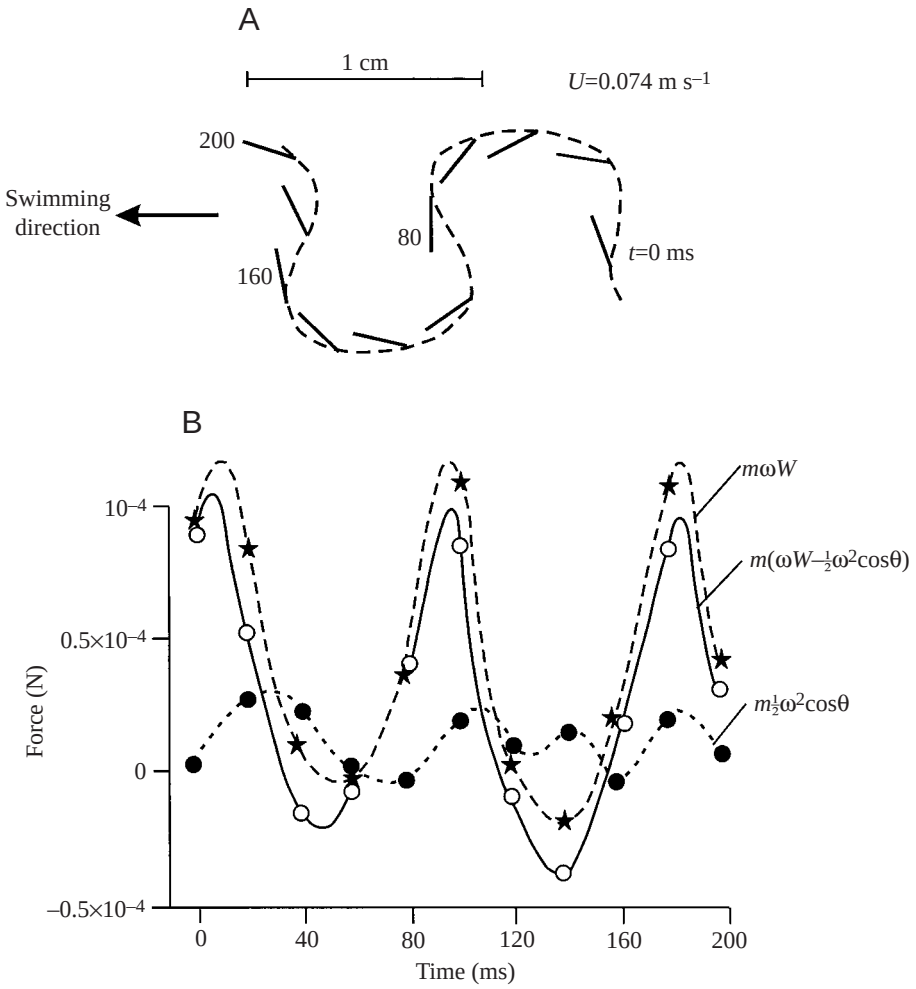


Fig. 5. (A) Path traced out by the caudal fin tip (dashed line) during a cycle of slow swimming movements. The bars on the swimming path indicate the orientation of the fin. $U$, instantaneous forward velocity; $t$, time. (B) Instantaneous force produced by the body wave (stars and dashed line), pressure force (filled circles and broken line) produced by the wake and resultant thrust force (open circles and solid line) calculated for the swimming path shown in A using the hydromechanical model. $m$, virtual mass per unit length of the body; $W$, lateral velocity of the tail tip; θ, the angle of inclination of tail fin to mean swimming line; ω, the perpendicular velocity of the tail tip.

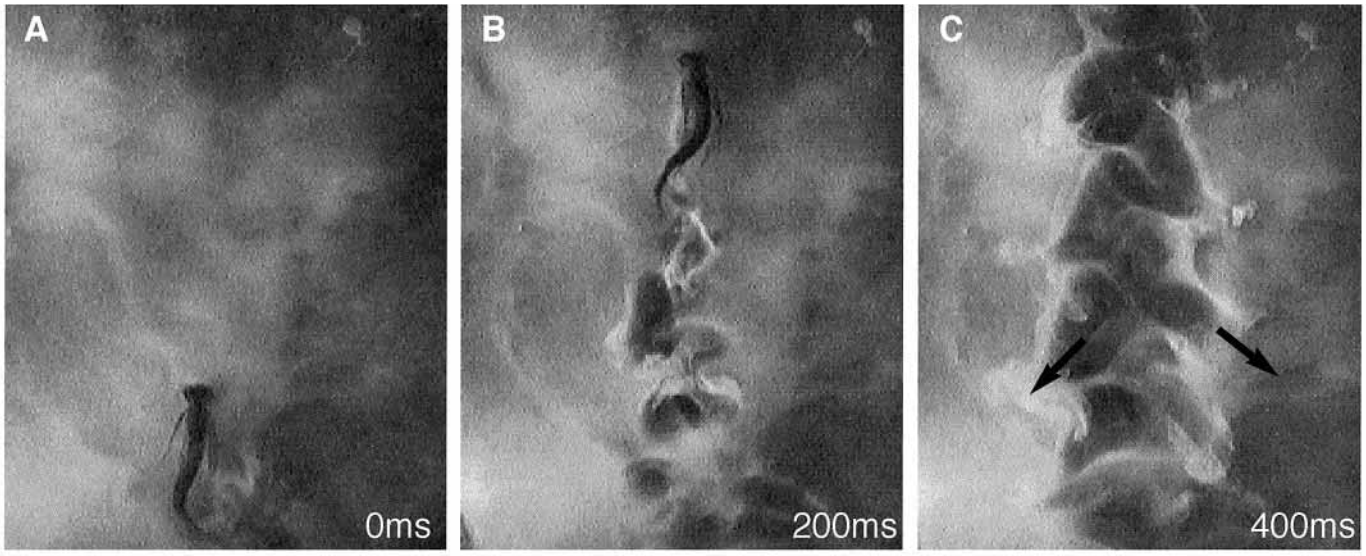


Fig. 6. Trail produced by the wake of a larva swimming in ‘fast’ mode (note the trailing legs) just above, but making no physical contact with, a layer of milk on the bottom of the container. The fully formed trail in the right-hand panel (C) indicates two series of jets, flowing alternately to the left and right of the mean swimming line and directed to the rear. The arrows indicate the axes of two of the jets.

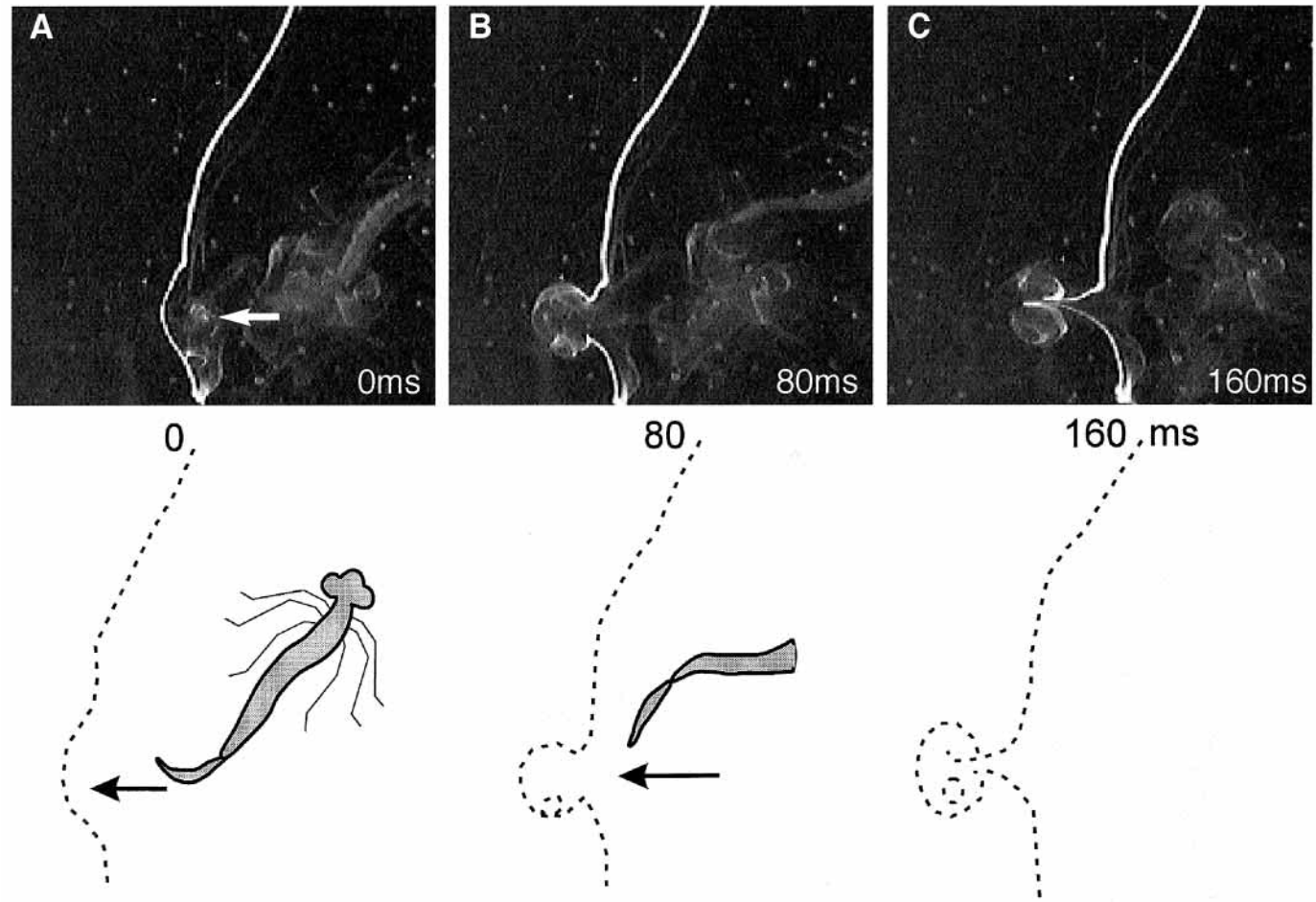


Fig. 7. Progressive visualisation of a discrete ring vortex shed from the tail fin at the end of a half-stroke. (A) The leading edge of the vortex is being outlined by the white streamer; the arrow indicates the direction of propagation of the vortex. (B) The vortex has passed through the streamer and is drawing dye into the trailing edge. (C) Dye has progressed beyond the ring plane, and the locations of the opposite cores of the vortex can be seen. Below, drawings of the main features shown in the videographic sequence.

almost directly to the side (Fig. 8B), and 40 ms after the start of the stroke a fully-formed vortex is about to be shed (Fig. 8C). Fig. 8D shows the shed vortex 160 ms later propagating along its momentum axis. This sequence is shown again in Fig. 4B and, by comparing it with Fig. 4A, it can be seen how, after vortex-shedding, the tail fin begins to straighten along the flexion line. This is also the point in the cycle when forward thrust production momentarily ceases (Fig. 5, 40 ms and 140 ms positions). These experiments also provided visual evidence of body-generated flows directly augmenting the flow generated by the tail. Fig. 4C shows successive body profiles at 20 ms intervals during a complete stroke of fast swimming lasting approximately 80 ms. Ahead of the tail fin tip, a portion of streamer became caught up in the motion of the body. As the larva moves forward, the undulatory wave of the body draws the dye steadily to the right (as indicated by the stars) so that by the completion of the tail fin stroke the dye joins the vortex now being released from the tail.

Hydrodynamic variables estimated from the measurements of jet velocity at the ring plane, momentum angle, vortex ring radius and vortex external diameter perpendicular to the ring plane are shown in the right hand column of Table 2. These are sufficiently close in value to those predicted from the hydromechanical model to give confidence to the conclusion that most of the momentum created in the water by the undulatory movements of body and tail fin was located within the observable wake structures, i.e. the vortices.

### *Starting manoeuvres*

Spontaneous, unprovoked swimming usually begins as a simple initiation of the head-to-tail wave that characterizes continuous swimming (Fig. 9A). The insect moves off in the direction in which the head was originally facing. The first two half-strokes of the tail fin are of small amplitude, and a correspondingly small vortex is shed at the end of the second half-stroke, but the first full-sized vortex coincides with the third half-stroke. The manner in which this, the first of a normal series of vortices, is augmented by the body flow is shown diagrammatically on the right of Fig. 9A. When swimming is provoked by an external stimulus, such as a light touch administered to the front of the body, a much more vigorous, asymmetric starting manoeuvre ensues. The body flexes rapidly to the opposite side from the stimulus, straightens out, then begins a series of normal undulations which carry it off at an angle to the original bearing and away from the stimulus. The turning angle can vary up to at least 160 °, depending on the strength of the original flexure (Fig. 9B,C). Since the turning manoevre is based on a single flexion/extension cycle, escape initiation can be as rapid as 100 ms. By depositing dye in the area of the body just before administering the shock, it was possible to visualise a jet of water, roughly in line with the axis of the concavity created by the original flexure, and directed opposite to the line of escape.

## Discussion

### *Morphology and kinematics*

The caudal fin of damsel-fly larvae is not exclusively a propulsive organ, but is also a gas-exchange surface liberally supplied with tracheal branches (Fig. 3B). A detailed consideration of the respiratory function of the tracheal plates is outside the scope of this study, although it is known that the plates are not essential for survival (Imms, 1964), and the author has observed specimens with one, two or all three plates missing, yet apparently thriving. Even in the latter case, larvae still attempt to swim by undulating the body, although these movements are extremely ineffective. To judge by the even distribution of tracheae within the plate, the whole surface would appear to be involved in the gas-exchange process, but the stiffening ribs in the base, the flexion line and the marginal hairs of the apical segment all seem to be specialisations related to the role of the plate as a propulsive organ. The three-lobed design of the fin, each lobe possessing some degree of independent movement in the median plane, lends a similar kind of radial mobility of fin elements to that found in ray-finned fishes.

Whilst the pectoral and pelvic fins of the swordfish *Xiphias gladius* are stiff and non-folding, those of other fishes such as Atlantic mackerel *Scomber scombrus* can be completely or partially folded against the body (Wardle, 1977). The pectoral fin of bluegill sunfish *Lepomis macrochirus*, like that of most teleosts, possesses a relatively stiff leading edge, which is under direct muscular control, and a passive posterior margin, features that help to determine the size, orientation and shape of ring vortices produced by the movements of the fin (Drucker and Lauder, 1999). Actively generated vortices of this nature are not found in swimming sturgeon, which has a stiff-rayed, non-flexible pectoral fin (Wilga and Lauder, 1999).

Although relative movement between the tracheal plates allows the height of the damsel-fly larval tail fin to be varied throughout the cycle, end-views of swimming larva offered no suggestion of any differences in the amplitude of the lateral excursion undergone by the individual plates. This question is of some importance since even the homocercal tail of fishes, with its external division into equal dorsal and ventral lobes, may not behave symmetrically throughout the stroke; the dorsal lobe undergoing a greater lateral excursion than the ventral lobe and, in the process, developing an upwardly directed or lifting force (Lauder, 2000). Since the damsel-fly larva is denser than water, a lifting force has to be generated to maintain level or upward swimming, although such a force has not been accounted for in this study. Even a small asymmetry in tail fin motion, with the dorsal plate undergoing a slightly larger lateral excursion than the other plates, might be sufficient to produce a slight downward tilt in the momentum axis of the vortex jet. There were only a few cases in which direct head-on or tail-on views of the swimming larva coincided with adequate visualisation of vortex production, but the impression given was that any downward inclination of the jet was small (less than 20 °). Clearly, this is an area where uncertainty remains and which would repay a more detailed investigation in a future study.

The serrations on the edges of the stiffening ribs in the base of the tracheal plates (Fig. 3B) may have some hydrodynamic function or, since they are essentially rather squat setae, they

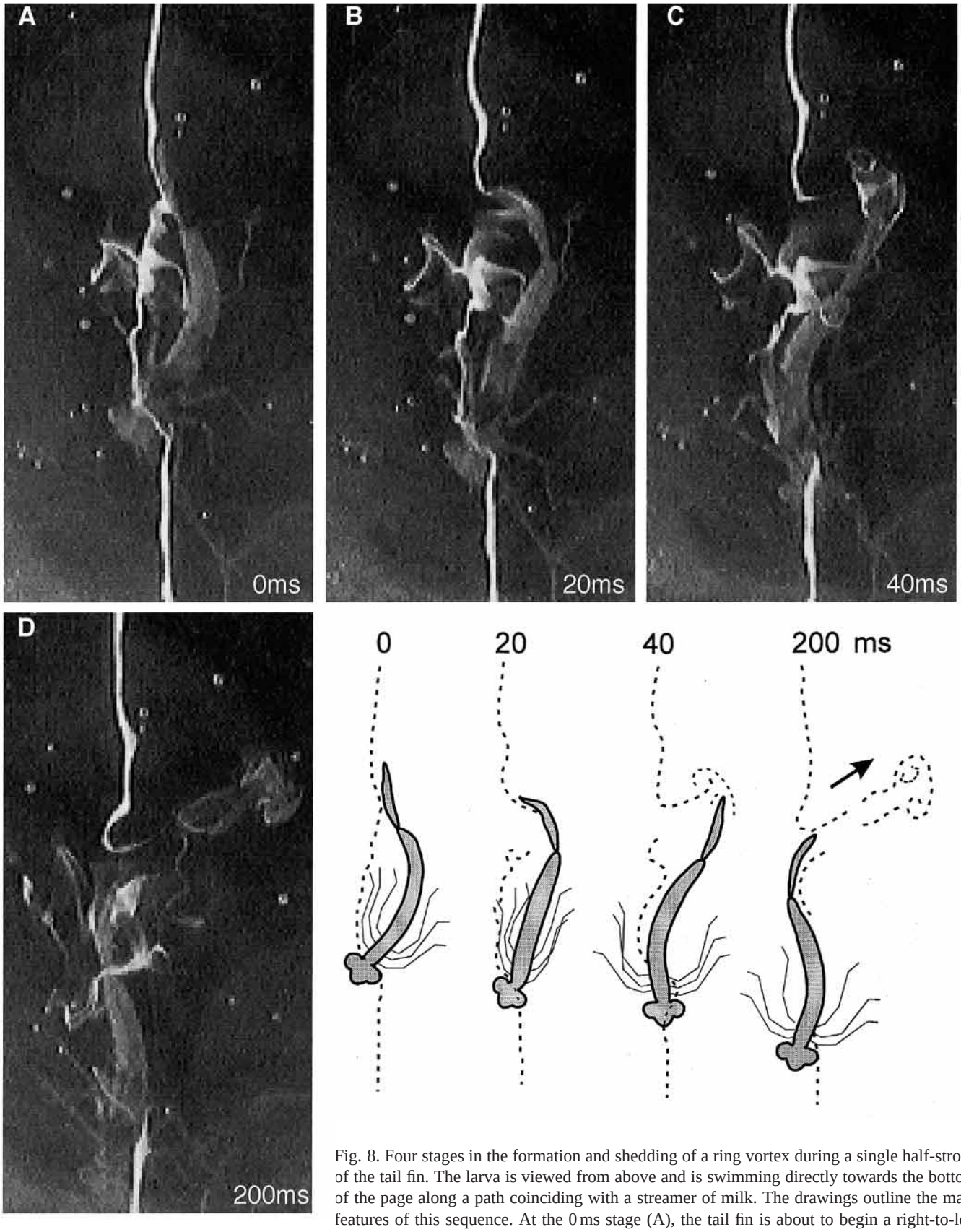


Fig. 8. Four stages in the formation and shedding of a ring vortex during a single half-stroke of the tail fin. The larva is viewed from above and is swimming directly towards the bottom of the page along a path coinciding with a streamer of milk. The drawings outline the main features of this sequence. At the 0 ms stage (A), the tail fin is about to begin a right-to-left swing and its right surface is in contact with the streamer. As the fin moves to the animal's left (B), it draws a current of water in its wake which, by the 40 ms stage (C), has rolled up into a ring vortex which is about to be shed. The vortex propagates to the side and to the rear in the direction of the arrow shown in the 200 ms drawing.

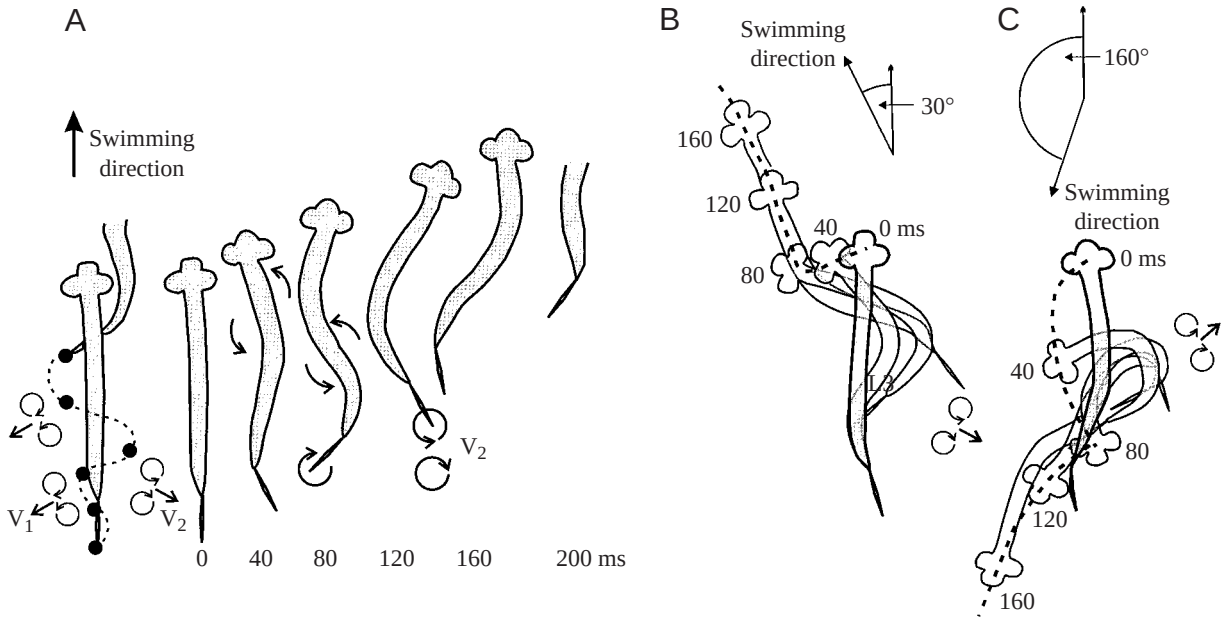


Fig. 9. Starting manoeuvres in *Enallagma cyathigerum* larva. (A) Start of normal swimming sequence. On the right is a series of body profiles at 40 ms intervals together with a scheme of the body and tail flows which contribute to the first full-sized vortex ($V_2$) in the swimming sequence. The path followed by the fin tip (filled circle) during the corresponding stages is shown on the left. A small vortex ($V_1$) is usually produced during the second half-stroke, but the first full-sized vortex is produced on the third half-stroke from the beginning of the manoeuvre. Note that the larva moves off on a heading parallel with the original orientation of the body. (B,C) Successive profiles, at 40 ms intervals, during two rapid-flex manoeuvres, one resulting in a turn of 30° (B) and the other 160° (C) away from the original heading of the body. In each case, the larva was reacting to a stimulus (light touch) from the right-hand side. As a result of a rapid flex away from this side followed by a rapid straightening of the body, a thrust jet is produced on the right-hand side, the direction of which is approximately opposite to the line of travel of the body out of the turn.

may be purely sensory. In speculating on their role, parallels could be drawn with similar microarchitectural adornments of propulsive organs such as the leading-edge serrations of dragonfly wings (Newman et al., 1977) or the finlets lying upstream of the caudal fin of scombroid fish (Nauen and Lauder, 2000). The former may enhance the transition to turbulence as air flows over the wing whilst, in the case of fish finlets, there is experimental evidence that they help channel flow longitudinally into the vortex forming at the tail. In both these cases, however, the operating Reynolds numbers are much higher than those experienced in the damsel-fly larval tail fin. This, again, is an area where microstructure suggests possible function but only direct observation, assisted perhaps by modelling, can supply any answers. A possible sensory role of the setae would be more difficult to investigate, although it may be significant that their location along the ribs would be ideal for detecting bending stresses within the fin base.

The speed of damsel-fly larvae swimming in ‘fast’ mode ($0.15\,m\,s^{-1}$) is less than that predicted for a fish of comparable body length swimming either continuously or in bursts (in both cases, approximately $0.25\,m\,s^{-1}$) (see fig. 10 in Wu, 1977). However, since 2 cm is close to the lower size limit available for data on swimming fish, comparisons may be misleading. The mean stroke amplitude of the tail fin tip of the five individuals listed in Table 2 was 0.41 BL, considerably higher than the average figure in fish (0.2–0.23 BL) (Hunter and Zweifel, 1971). In contrast, the height of the caudal fin (0.13–0.17 BL) is small compared with that of teleosts (0.23 L) (Webb, 1977). These factors may be related, the relatively high amplitude of the body undulation compensating for the relatively low added mass on the tail fin and abdomen.

Slow and fast swimming are not two extremes of a continuum but behaviourally and biomechanically distinct and alternative forms of locomotion. The rowing motion of the legs during slow swimming bears the hallmarks of walking in terms of both metachronicity and the cycle of retraction/extension and protraction/flexion. The limb kinematics are consistent with the generation of a net force in the forward direction due to the increased effective length of the leg during the backstroke. In the energy budget of the larva, this gain must be offset against the overall increase in drag *per se* that inevitably results from active deployment of the legs. Whilst emphasising the propulsive role of the legs in slow swimming, it must not be overlooked that they may also play a part in stabilising the body against roll. Similarly, the fact that the legs appear to be trailed ‘passively’ through the water during fast swimming does not necessarily mean that the leg muscles are ‘relaxed’. In resting larvae, the legs are held to the side of the body, with the joints in the partially flexed position. This is also the position to which the legs are restored as soon as fast swimming ceases. So, although the legs appear to be passively trailed during fast swimming, they may in fact be actively held in the fully extended, maximally retracted position.

Damsel-fly larvae are not exceptional amongst aquatic

insects in possessing more than one modality of locomotion. In addition to their familiar 'lashing' style of locomotion, feeding mosquito larvae regularly employ a much slower gliding form of swimming in which the body is propelled by the mouthparts (Brackenbury, 2001b), and chironomid larvae and pupae possess between them at least five distinct forms of swimming each tailored to different environmental circumstances (Brackenbury, 2000).

The rapid-flexure manoeuvre of startled larvae (Fig. 9B) is remarkably similar, both kinematically and hydrodynamically, to the fast C-start of fish. C-starting is a means of procuring a rapid escape from threat and involves turning angles up to 180 ° either side of the body. Although the C-start can be divided kinematically into a preparatory stroke (the rapid flex), a propulsive stroke (extension) and finally a variable stage consisting of continuous or coasting swimming (see Domenici and Blake, 1997), recent flow visualisation studies suggest that the flex and unflex are a continuum in the production of a thrust jet (Wolfgang et al., 1999). Rapid curvature of the backbone into a C-shape draws fluid into the C-shaped cavity as two oppositely signed vortices develop simultaneously around the head and tail ends of the body. Rapid straightening then leads to the body-generated vortices being shed into the wake as a thrust jet which drives the fish in the direction of the initial flexure. This analysis of events applies equally to the rapid-flexure manoevre of damsel-fly larvae, including the direction of the resultant thrust jet. Behaviour immediately following the turn may also vary in larvae, just as it does in C-starting fish. Usually, turning is the prelude to rapid swimming in the new direction, but in other instances the larva simply turns on the spot without further sequel.

### *Hydrodynamics*

With whole-body Reynolds numbers of approximately $3\times10^{-3}$, fast-swimming damsel-fly larvae would be expected to generate most of their thrust from inertial rather than viscous forces (Wu, 1977). In preparing the ground for his classic bulk-momentum model of undulatory swimming in fish, Lighthill (1971) argued that the undulatory motion of elongated invertebrates is probably best studied by resistive, not reactive, theory since the circular cross section of the body of many of these worm-like organisms is ill-fitted to the enhancement of virtual mass effects. Whilst there is strong evidence that undulating nematodes (Gray and Lissman, 1964) and the wormlike larvae of ceratopogonid flies (Nachtigall, 1961) propel themselves using viscous forces, the ribbon-like shape of the body of leeches, for example, which also swim sinusoidally (Kristan et al., 1982), could promote virtual mass effects. Even chaetognaths, which undulate at Reynolds numbers of 100 or less, generate some force through water acceleration according to the hydrodynamic analysis of Jordan (1992). Flow field measurements on swimming culicid larvae and pupae with Reynolds numbers of approximately $10^3$ show that virtually all the force needed to drive the body forwards can be accounted for in the momentum of the wake (Brackenbury, 2001a). Although culicids are not undulatory swimmers, but perform large-amplitude side-to-side flexural movements of the body, the findings do at least show that inertial forces can be dominant in invertebrate swimming even at low to intermediate Reynolds numbers.

Swimming damsel-fly larvae resemble culicids in generating a relatively simple wake that consists of a double row of discrete vortices which convect away from the mid-line and constitute the bulk of the visible wake structure. Neither insect produces an aft-flowing jet. In both the culicid study and the present study, vortex momentum has been estimated by assuming that the vortices are small-cored, although this could not be confirmed by detailed measurements. In the present study, the further assumption is made that the fluid velocity distribution down the centre line of the vortex is pyramidal, peaking at the ring plane. This is approximately what would be expected of a ring vortex and is in accord with the measurements on culicid vortices.

The wake structure of damsel-fly larvae differs from that of fish swimming continuously by the use of the caudal fin, which consists of a double row of stationary vortices linked into a chain, with a caudally directed jet zig-zagging through them (Muller et al., 1997; Wolfgang et al., 1999). A reverse Karman vortex street of this nature is not typical of all fish: intermittent swimmers, such as *Brachydanio rerio* (McCutchen, 1977), and pectoral fin swimmers at low speeds (Drucker and Lauder, 1999) generate discrete, unlinked vortices. Especially forceful, high-impulse ring vortices shed at right angles to the body have been measured during turning manoeuvres in a pectoral fin swimmer (Drucker and Lauder, 2000). The latter authors allude to the errors that can result in the calculation of wake energies from incorrectly modelled wake structures, a point also made by Spedding (1987), who invoked hidden wake structures as a possible explanation for the apparent momentum deficit in the wake of flying birds.

Particle image velocimetry involves careful reconstruction of three-dimensional flow structures from planar sections and measures velocities with great accuracy. It is possibly the only technique available for the reconstruction of complex wakes. When the principal wake structures are discrete vortices which move laterally, leaving little axial disturbance to the water immediately behind the swimming animal, a relatively simple technique such as that used in the present study can produce good, quantitative data. As the author has confirmed in preliminary observations on small fish, such a technique is unsuitable for visualising wakes with a complex mid-line architecture. The principal source of potential error in the present study lies in the estimate of vortex jet velocity at the ring plane, which ideally should be measured at the instant when the vortex is shed. Since it requires a finite time (20–40 ms) for the dye to be drawn into the trailing edge of the vortex and towards the ring plane, this condition obviously cannot be met stringently. However, any resulting error would be in the direction of underestimating, not overestimating, vortex momentum.

The main conclusion to be drawn from the closeness of the estimates of thrust production from the hydromechanical model and flow field measurements (Table 2) is that there is

little or no hidden momentum in wake structures external to the observed ring vortices. The agreement between the estimates also suggests that the large-amplitude, elongate-body model is appropriate for the study of undulatory motion in an invertebrate with the size and swimming speed of these larvae. However, the results do not resolve the question of the possible involvement of viscous forces in thrust production since the model specifically excludes these. The only way of establishing whether a force balance truly exists in a swimming organism is to measure both thrust and drag in the same experiments, although the study by Drucker and Lauder (1999) appears to be the only one to date to have done this.

Finally, although damsel-fly larvae appear to be relatively slow swimmers compared with small fish, this does not mean that their locomotion is less efficient. The estimated Froude (propulsive) efficiency from both the hydromechanical model and the wake momentum measurements (Table 2) is approximately 66 % compared with values of 70–80 % in fish (Alexander, 1999). A greater absolute swimming speed in a fish compared with a similarly sized invertebrate could simply indicate a higher mass-specific muscle power output.

I am grateful to Adrian Newman for help with videographics, Dee Hughes for the artwork and Emma Snook for typing the manuscript. I am also grateful to staff at the EPSRC Engineering Instrument Pool, Oxford for helpful advice on videographic recording.

## References

**Alexander, R. McN.** (1999). *Energy for Animal Life*. Oxford: Oxford University Press.

**Blickan, R., Krick, C., Zehren, D. and Nachtigall, W.** (1992). Generation of a vortex chain of a subundulatory swimmer. *Naturwissenschaften* **79**, 220–221.

**Brackenbury, J. H.** (1999). Regulation of swimming in the *Culex pipiens* (Diptera, Culicidae) pupa: kinematics and locomotory trajectories. *J. Exp. Biol.* **202**, 2521–2529.

**Brackenbury, J. H.** (2000). Locomotory modes in the larva and pupa of *Chironomus plumosus* (Diptera, Chironomidae). *J. Insect Physiol.* **46**, 1517–1527.

**Brackenbury, J. H.** (2001a). The vortex wake of the free-swimming larva and pupa of *Culex pipiens* (Diptera). *J. Exp. Biol.* **204**, 1855–1867.

**Brackenbury, J. H.** (2001b). Locomotion through use of the mouth brushes in the larva of *Culex pipiens* (Diptera: Culicidae). *Proc. R. Soc. Lond. B* **268**, 101–106.

**Chia, F. S., Buckland-Nicks, J. and Young, C. M.** (1984). Locomotion of marine invertebrate larvae: a review. *Can. J. Zool.* **62**, 1205–1222.

**Domenici, P. and Blake, R. W.** (1997). The kinematics and performance of fish fast-start swimming. *J. Exp. Biol.* **200**, 1165–1178.

**Drucker, E. G. and Lauder, G. V.** (1999). Locomotor force on a swimming fish: three-dimensional vortex wake dynamics quantified using digital particle image velocimetry. *J. Exp. Biol.* **202**, 2393–2412.

**Drucker, E. G. and Lauder, G. V.** (2000). Wake dynamics and fluid forces of turning maneuvers in sunfish. *J. Exp. Biol.* **204**, 431–442.

**Ellington, C. P.** (1984). The aerodynamics of hovering insect flight. V. A vortex theory. *Phil. Trans. R. Soc. Lond. B* **305**, 115–144.

**Gray, J. and Lissman, H. W.** (1964). The locomotion of nematodes. *J. Exp. Biol.* **41**, 135–154.

**Grodnitsky, D. L.** (1999). *Form and Function in Insect Wings.* Baltimore, London: The John Hopkins University Press.

**Hoyle, E.** (1976). Arthropod walking. In *Advances in Behavioural Biology, Neural Control of Locomotion*, vol. 18 (ed. R. M. Herman, S. Grillner, P. S. G. Stein and D. G. Stuart), pp. 137–177. New York: Plenum.

**Hughes, E. M.** (1974). Locomotion. In *The Physiology of Insecta*, vol. III (ed. M. Rockstein), pp. 335–379. New York: Academic Press.

**Hunter, J. R. and Zweifel, J. R.** (1971). Swimming speed, tail beat frequency, tail beat amplitude and size in jack mackerel, *Trachurus symmetricus*, and other fishes. *Fish. Bull.* **69**, 253–266.

**Imms, A. D. C.** (1964). *A General Textbook of Entomology.* London: Methuen & Co. Ltd.

**Jordan, C. E.** (1992). A model of rapid-start swimming at intermediate Reynolds numbers: undulatory locomotion in the chaetognath *Sagitta elegans*. *J. Exp. Biol* **163**, 119–137.

**Kristan, W. B., McGirr, S. J. and Simpson, G. V.** (1982). Behavioural and mechanosensory neurone responses to skin stimulation in leeches. *J. Exp. Biol.* **96**, 143–160.

**Lauder, G. V.** (2000). Function of the caudal fin during locomotion in fishes: kinematics, flow visualization and evolutionary patterns. *Am. Zool.* **40**, 101–122.

**Lighthill, M. J.** (1969). Hydrodynamics of aquatic animal locomotion. *A. Rev. Fluid Mech.* **1**, 413–446.

**Lighthill, M. J.** (1970). Aquatic animal propulsion of high hydrodynamic efficiency. *J. Fluid Mech.* **44**, 265–301.

**Lighthill, M. J.** (1971). Large-amplitude elongated-body theory of fish locomotion. *Proc. R. Soc. Lond. B* **179**, 125–138.

**McCutchen, C. W.** (1977). Froude propulsive efficiency of a small fish, measured by wake visualization. In *Scale Effects in Animal Locomotion* (ed. T. J. Pedley), pp. 339–363. London, New York, San Francisco: Academic Press.

**Muller, V. K., Van den Heuvel, B. L. F., Stamhuis, E. J. and Videler, J. J.** (1997). Fish foot-prints: morphometrics and energetics of the wake behind a continuously swimming mullet (*Chelon labrosus* Risso). *J. Exp. Biol.* **200**, 2893–2900.

**Nachtigall, W.** (1961). Zur Locomotionsmechanik schwimmender Dipterenlarven. I. Mitteilung: Schwimmen ohne Ruderorgane: Ceratopogoniden und Chironomiden. *Z. Vergl. Physiol.* **44**, 509–522.

**Nachtigall, W.** (1962). Zur Locomotionsmechanik Dipterenpuppen. *Z. Vergl. Physiol.* **45**, 463–474.

**Nachtigall, W.** (1963). Zur Locomotionsmechanik schwimmender Dipterenlarven. Mitteilung: Schwimmen mit Ruderorganen: Culicinen und Corethrinen. *Z. Vergl. Physiol.* **46**, 449–466.

**Nauen, J. C. and Lauder, G. V.** (2000). Locomotion of scombroid fishes: morphology and kinematics of the finlets of the chub mackerel *Scomber japonicus. J. Exp. Biol.* **203**, 2247–2259.

**Newman, B. G., Savage, S. B. and Schouella, D.** (1977). Model tests on a wing section of an *Aeschna* dragonfly. In *Scale Effects in Animal Locomotion* (ed. T. J. Pedley), pp. 445–477. London, New York, San Francisco: Academic Press.

**Rayner, J. M. V.** (1979). A vortex theory of animal flight. Part 1. The vortex wake of a hovering animal. *J. Fluid Mech.* **91**, 697–730.

**Rayner, J. M. V., Jones, E. and Thomas, A.** (1986). Vortex flow visualizations reveal change in upstroke function with flight speed in bats. *Nature* **321**, 162–164.

**Spedding, G. R.** (1986). The wake of a jackdaw (*Corvus monedula)* in slow flight. *J. Exp. Biol.* **125**, 287–307.

**Spedding, G. R.** (1987). The wake of a kestral (*Falco tinnunculus*) in flapping flight. *J. Exp. Biol.* **127**, 59–78.

**Spedding, G. R., Rayner, J. M. V. and Pennycuick, C. J.** (1984). Momentum and energy in the wake of a pigeon (*Columba livia)* in slow flight. *J. Exp. Biol.* **111**, 81–102.

**Stokes, M. D.** (1997). Larval locomotion of the lancelet *Branchiostoma floridae. J. Exp. Biol.* **200**, 1661–1680.

**Videler, J. B.** (1993). *Fish Swimming*. London: Chapman & Hall.

**Wardle, C. S.** (1977). Effects of size on the swimming speeds of fish. In *Scale Effects in Animal Locomotion* (ed. T. J. Pedley), pp. 299–313. London, New York, San Francisco: Academic Press.

**Webb, P. W.** (1977). Effects of size on performance and energetics of fish. In *Scale Effects in Animal Locomotion* (ed. T. J. Pedley), pp. 315–331. London, New York, San Francisco: Academic Press.

**Wilga, C. D. and Lauder, G. V.** (1999). Locomotion in sturgeon: function of the pectoral fins. *J. Exp. Biol.* **202**, 2413–2432.

**Wolfgang, M. J., Anderson, J. M., Grosenbaugh, M. A., Yue, D. K. P. and Triantophyllou, M. S.** (1999). Near-body flow dynamics in swimming fish. *J. Exp. Biol.* **202**, 2302–2327.

**Wu, T. Y.** (1977). Introduction to the scaling of aquatic animal locomotion. In *Scale Effects in Animal Locomotion* (ed. T. J. Pedley), pp. 203–232. London, New York, San Francisco: Academic Press.